BRAIN
ORIGINAL ARTICLE

Widespread white matter oedema in subacute COVID-19 patients with neurological symptoms

Alexander Rau,[1,†] Nils Schroeter,[2,†] Ganna Blazhenets,[3] Andrea Dressing,[2,4] Lea I. Walter,[2] Elias Kellner,[5] Tobias Bormann,[2,4] Hansjörg Mast,[1] Dirk Wagner,[6] Horst Urbach,[1] Cornelius Weiller,[2,4] Philipp T. Meyer,[3] Marco Reisert[5,7] and Jonas A. Hosp[2]

[†]These authors contributed equally to this work.

While neuropathological examinations in patients who died from COVID-19 revealed inflammatory changes in cerebral white matter, cerebral MRI frequently fails to detect abnormalities even in the presence of neurological symptoms. Application of multi-compartment diffusion microstructure imaging (DMI), that detects even small volume shifts between the compartments (intra-axonal, extra-axonal and free water/CSF) of a white matter model, is a promising approach to overcome this discrepancy.

In this monocentric prospective study, a cohort of 20 COVID-19 inpatients (57.3 ± 17.1 years) with neurological symptoms (e.g. delirium, cranial nerve palsies) and cognitive impairments measured by the Montreal Cognitive Assessment (MoCA test; 22.4 ± 4.9; 70% below the cut-off value <26/30 points) underwent DMI in the subacute stage of the disease (29.3 ± 14.8 days after positive PCR). A comparison of whole-brain white matter DMI parameters with a matched healthy control group ($n = 35$) revealed a volume shift from the intra- and extra-axonal space into the free water fraction (V-CSF). This widespread COVID-related V-CSF increase affected the entire supratentorial white matter with maxima in frontal and parietal regions. Streamline-wise comparisons between COVID-19 patients and controls further revealed a network of most affected white matter fibres connecting widespread cortical regions in all cerebral lobes. The magnitude of these white matter changes (V-CSF) was associated with cognitive impairment measured by the MoCA test ($r = –0.64$, $P = 0.006$) but not with olfactory performance ($r = 0.29$, $P = 0.12$). Furthermore, a non-significant trend for an association between V-CSF and interleukin-6 emerged ($r = 0.48$, $P = 0.068$), a prominent marker of the COVID-19 related inflammatory response. In 14/20 patients who also received cerebral ^{18}F-FDG PET, V-CSF increase was associated with the expression of the previously defined COVID-19-related metabolic spatial covariance pattern ($r = 0.57$; $P = 0.039$). In addition, the frontoparietal-dominant pattern of neocortical glucose hypometabolism matched well to the frontal and parietal focus of V-CSF increase.

In summary, DMI in subacute COVID-19 patients revealed widespread volume shifts compatible with vasogenic oedema, affecting various supratentorial white matter tracts. These changes were associated with cognitive impairment and COVID-19 related changes in ^{18}F-FDG PET imaging.

1 Department of Neuroradiology, Medical Center – University of Freiburg, Faculty of Medicine, University of Freiburg, Freiburg, Germany
2 Department of Neurology and Clinical Neuroscience, Medical Center – University of Freiburg, Faculty of Medicine, University of Freiburg, Freiburg, Germany
3 Department of Nuclear Medicine, Medical Center – University of Freiburg, Faculty of Medicine, University of Freiburg, Freiburg, Germany

Received November 01, 2021. Revised December 30, 2021. Accepted January 23, 2022

4 Freiburg Brain Imaging Center, Medical Center – University of Freiburg, Faculty of Medicine, University of Freiburg, Freiburg, Germany
5 Department of Medical Physics, Medical Center – University of Freiburg, Faculty of Medicine, University of Freiburg, Freiburg, Germany
6 Department of Internal Medicine, Medical Center – University of Freiburg, Faculty of Medicine, University of Freiburg, Freiburg, Germany
7 Department of Stereotactic and Functional Neurosurgery, Medical Center – University of Freiburg, Faculty of Medicine, University of Freiburg, Freiburg, Germany

Correspondence to: Jonas A. Hosp MD
University Medical Center
Freiburg Department of Neurology and Neuroscience
Breisacher Str. 64, 79106 Freiburg, Germany
E-mail: jonas.hosp@uniklinik-freiburg.de

Keywords: diffusion microstructure imaging; COVID-19; cognition; ^{18}F-FDG PET; Montreal Cognitive Assessment

Abbreviations: DMI =diffusion microstructure imaging; MoCA =Montreal Cognitive Assessment; V-CSF =free water/CSF fraction; V-extra =extra-axonal volume fraction; V-intra =intra-axonal volume fraction

Introduction

Neurological complications[1] and long-term consequences[2] of an acute respiratory syndrome coronavirus 2 (SARS-CoV-2/COVID-19) infection are widely recognized. In a recent study, we described an impairment of frontoparietal cognitive functions in subacute COVID-19 inpatients accompanied by a frontoparietal-dominant neocortical glucose hypometabolism revealed by ^{18}F-FDG PET.[3] Insights into the potential pathophysiological basis of this phenomenon came from recent neuropathological studies investigating microstructural changes within brains of patients who died from COVID-19.[4–6] Here, activation of microglia and astrocytes has been detected particularly in the brainstem and cerebellum. Interestingly, neuropathological changes involved the white more than the grey matter. Thus, we hypothesized that an inflammatory affection of white matter fibres could compromise the function of connected cortical areas—as witnessed by reduced neocortical glucose metabolism and cognitive impairments as measured by the Montreal Cognitive Assessment (MoCA).[3]

On structural MRI, overall findings in acute and subacute COVID-19 patients are heterogeneous and mainly comprise leukoencephalopathy and microhaemorrhages, neurovascular complications (thromboses and infarctions) or inflammatory syndromes (e.g. acute necrotizing encephalitis).[7,8] However, structural MRI frequently fails to detect seminal changes in COVID-19 patients with neurological symptoms.[9,10] Particularly, MRI-derived *in vivo* evidence of inflammatory white matter alterations as seen in post-mortem histopathological studies is widely lacking.[11] To bridge the gap between classic *in vivo* MRI and post-mortem histology, the application of multi-compartment diffusion microstructure imaging (DMI) could be a promising approach to capture COVID-19-related changes in white matter meso-/microstructure.[12] Technically, DMI is based on advanced multi-shell diffusion protocols that allow distinguishing different anatomical compartments by their diffusion properties. Whereas 'free' water molecules randomly move without restriction, water molecules in neuronal processes or the extracellular matrix are aligned by organelles and membranes. This led to the delineation of a standard white matter model[13–15] consisting of three components: (i) the free water/CSF fraction (V-CSF); (ii) the intra-axonal volume fraction (V-intra) with almost one-dimensional molecule diffusion due to tight membrane borders; and (iii) the extra-axonal volume fraction (V-extra) representing the extra-axonal cellular compartment and the extracellular matrix, characterized by restricted diffusion. In contrast to classical diffusion tensor imaging (DTI) indices, the DMI diffusivity parameters offer more specific and interpretable measures of tissue integrity. An increase of V-CSF has been linked to neurodegeneration in amyotrophic lateral sclerosis[16] or to vasogenic oedema in traumatic brain injury.[17] In turn, a decrease of V-intra is a sensitive indicator of reduced white matter fibre integrity caused by chronic inflammation[18] or mechanical stress.[19] To decouple the contribution of these components to DMI-signals and allow the estimation of compartment-specific volume fractions, we recently introduced a supervised machine learning approach in the form of a Bayesian estimator.[14] Here, we applied this approach to assess and analyse DMI signals to detect white matter alterations in a monocentric cohort of 20 subacute COVID-19 inpatients with neurological symptoms. Parts of this cohort have been previously described in the aforementioned study showing frontoparietal-dominant neocortical glucose hypometabolism and cognitive impairments related to COVID-19.[3] Moreover, we assessed whether DMI signals were related to the clinical parameters MoCA, olfactory performance as well as the inflammatory marker interleukin-6 (IL-6). As 14 of 20 patients also underwent ^{18}F-FDG PET imaging, we further investigated the association between DMI-parameters and the expression of the COVID-19-related spatial covariance pattern of cerebral glucose metabolism.

Material and methods

Study participants and clinical outcomes

In the present study, we report an analysis of MRI and ^{18}F-FDG PET data derived from a prospective monocentric register (Neuro-COVID-19; for details see Hosp *et al.*[3]). The local ethics committee approved this study (EK 211/20) and all subjects gave written informed consent in accordance with the Declaration of Helsinki and its later amendments. The register enrolled patients with reverse transcription polymerase chain reaction (rt-PCR) confirmed

SARS-CoV-2 infection, at least one novel neurological symptom developed under COVID-19 and required inpatient treatment at the Department of Internal Medicine of the University Hospital Freiburg between 20 April 2020 and 10 May 2021. Exclusion criteria were any pre-existing neurodegenerative disorders and age <18 years. Imaging was performed as soon as infectivity was no longer present according to the in-house guidelines of the University Hospital Freiburg. Twenty-three patients of our cohort received a cranial MRI. Of these, three patients had to be excluded due to changes that would have interfered with further data processing: signs of widespread cerebral amyloid angiopathy (one male, 77 years), MRI pattern of normal pressure hydrocephalus (one male, 75 years) and previously known unilateral white matter gliosis in the deep watershed (one female, 61 years).

Patients were examined and surveyed by board certified (A.D., J.H.) or experienced (>6 years of training, N.S.) neurologists. Cognitive functions were assessed with the German version of the MoCA (version 7.1, www.mocatest.org).[20] The highest possible global MoCA score is 30 with higher scores indicating better performance, the cut-off score for cognitive impairment was defined as < 26.[20] Correction for years of education (YoE) was performed (+1 point in case of ≤12 YoE). MoCA domain scores were calculated as means of single item scores and comprise subscores for orientation (spatial and temporal orientation), attention (digit span, letter A tapping and subtraction), executive function (trail making, abstraction and word fluency), visuoconstructive function (cube copying and clock drawing), language (naming, sentence repetition), and memory (delayed word recall). Domain scores were not adjusted for years of education. In a subset of 13 patients, a comprehensive neuropsychological test battery was performed (Supplementary material). Olfaction was assessed using Burghart-Sniffin'-Sticks® (Burghart Messtechnik GmbH), an established screening test of olfactory performance.[21] Ammonium was used to assess trigeminal function (normosmia: 11–12 correctly identified odours; hyposmia: 7–10 correct odours; anosmia: ≤6 correct odours). To evaluate the intensity of the systemic inflammatory response in the disease course prior to MRI, the peak value of the cytokine IL-6, one of the most established markers for the SARS-CoV-2 related inflammation,[22] was measured in a subset of 17/20 patients.

Cerebral MRI

MRI acquisition

MRI was performed with a 3 T scanner (MAGNETOM Prisma, Siemens Healthcare) with a 64-channel head and neck coil. T_1-weighted images were acquired with a 3D magnetization-prepared 180° radio-frequency pulses and rapid gradient-echo (MP-RAGE) sequence (repetition time: 2500 ms, echo time: 2.82 ms, flip angle: 7°, inversion time = 1100 ms, GRAPPA factor = 2, 1.0 mm isotropic voxels, 192 contiguous sagittal slices). The DTI/DMI sequence was acquired with the following parameters: axial orientation, 42 slices, voxel size $1.5 \times 1.5 \times 3$ mm^3, repetition time = 2800 ms, echo time = 88 ms, bandwidth 1778 Hz, flip angle 90°, SMS factor 3, 15 non-diffusion weighted images, 2×58 images with b-factors 1000 and 2000 s/mm^2.

Calculation of DMI parameters

Data processing was implemented within our in-house postprocessing platform NORA (www.nora-imaging.org). Preprocessing of diffusion-weighted images included a denoising step[23] followed by correction of the Gibbs-ringing artefacts[24] and final upsampling to isotropic resolution. Microstructural diffusion metrics were estimated using a Bayesian approach[14] to determine the three components of a standard white matter model[13,14,25]: (i) the V-CSF in that molecule randomly move at the distance of their diffusion length (in the range of tenth of μm); (ii) the V-intra with almost one-dimensional molecule diffusion due to tight membrane borders; and (iii) the V-extra, characterized by an intermediate constraint to molecule diffusion representing the extra-axonal cellular compartment and the extracellular matrix. Technically, different approaches have been established to allow the estimation of compartment-specific volume fractions from the diffusion MRI (dMRI) signals. Relying on maximum likelihood estimation, the neurite orientation dispersion and density imaging (NODDI) technique is the most established one.[12] However, the NODDI approach requires stabilization by hard *a priori* constraints and is hampered by computing times of several hours for one dataset. In contrast, our supervised machine learning approach in the form of a Bayesian estimator relaxes the hard constraints by using assumed smooth and biophysically motivated prior distributions.[14] With processing times of only 6 min per dataset, extraction of mesoscopic diffusivity parameters is applicable for daily clinical routine. To corroborate the results of our model, we also extracted diffusivity parameters using the accelerated microstructure imaging via convex optimization (AMICO)-NODDI, a regularized version of NODDI that also allows fast processing times due to the linearization of fitting procedures (https://github.com/daducci/AMICO).[26] T_1-weighted imaging datasets were automatically segmented into white matter, grey matter and CSF using CAT12 (http://www.neuro.uni-jena.de/cat/) and diffusion MRI (dMRI) images were co-registered to the T_1-weighted images. Validity of co-registrations between dMRI images, T_1-weighted and binary masks was manually confirmed. Further, quality control was performed by visually inspecting each individual DMI map and CAT12 segmentation.

Spatial normalization and voxel-wise comparisons

To investigate the spatial distribution of COVID-19-related changes on dMRI parameters by voxel-wise analysis, images were spatially normalized by CAT12 using the DARTEL (diffeomorphic anatomical registration using the exponentiated lie algebra) method.[27] The diffeomorphic warp was used to transfer the quantitative dMRI maps to the Montreal Neurological Institute (MNI) space. Images were smoothed with a 3-mm full-width at half-maximum (FWHM) Gaussian kernel. The dataset of COVID-19 patients was compared to an in-house control collective of 35 healthy subjects [18 males, 17 females; mean age 51.8 years; standard deviation (SD) = 17.3; range: 21–81 years; further characteristics are given in the Supplementary material] that did not significantly differ in sex (χ^2, $P = 0.29$) and age (*t*-test, $P = 0.26$) with unimpaired performance in MoCA and no neurological deficit in physical examination. As implemented in the statistical parametric mapping voxel-based morphometry (SPM-VBM) 8-Toolbox, voxel-based group comparison of the DMI parameter V-CSF was performed using a parametric multiple regression model. For T_1-weighted images, modulation was performed by multiplying the partitioned images by the relative volumes (i.e. the Jacobian determinants of the deformation field). For DMI parameters, no modulation was applied, i.e. all values were preserved. Only white matter was taken into account, as the three-compartment biophysical model was developed and validated for white matter tissue. To better differentiate between

diffusion-related effects and effects that are already visible in a T_1-weighted anatomical scan (typically hypo-intense white matter abnormalities such as microangiopathic/gliotic lesions) or any pre-existing volumetric effects, the information of the tissue probability maps (i.e. 'tissue probability value') was derived by CAT12 and implemented into the model as covariate on a voxel-by-voxel level. Additionally, this approach minimized the risk that partial volume effects at the border of grey and white matter may contribute to the effect. Moreover, 'age' and 'sex' served as nuisance covariates. Voxel-wise analyses were carried out as group comparisons between COVID-19 patients and healthy control subjects.

Streamline-wise comparisons

To further investigate the white matter networks that were especially affected by COVID-19-related V-CSF changes and corresponding cortical termination areas, we considered a normative structural connectome in MNI space based on diffusion data of 200 subjects from the Human Connectome Project database (www.humanconnectome.org). From the parameter sets provided by the toolbox,[28] we utilized the 'sparse' reconstruction setting for our analyses, which results in ~5000 streamlines. Individual V-CSF contrast images were first warped from subject space into MNI space as described above. Then, the V-CSF values of every voxel attached to a particular streamline were averaged to obtain a streamline-specific value. Subsequently, whole connectome streamline-wise comparisons between COVID-19 patients and healthy controls were performed using a parametric multiple regression model with 'age' and 'sex' as nuisance factors. To assess the corresponding white matter areas covered by selected streamlines, fibres in white matter as provided by CAT 12 were rendered on a grid of a resolution $2.5 \times 2.5 \times 2.5$ mm^3 by trilinear interpolation. Of the resulting maps, the area containing the lowest 33% of fibre density values was cropped to reduce noise and the output was converted to binary masks. The anatomical allocation of white matter tracts was performed secondarily by using a probabilistic atlas.[29]

^{18}F-FDG PET imaging

PET emission data were acquired 50 min after intravenous injection of 215 ± 12 MBq ^{18}F-FDG for 10 min as described elsewhere.[3,30] ^{18}F-FDG PET scans were spatially normalized to an in-house ^{18}F-FDG PET template in MNI space and smoothed with an isotropic Gaussian kernel of 10 mm FWHM. The topographic profile rating algorithm[31] of the ScAnVP software was employed to derive each individual's pattern expression score (PES) of the previously established COVID-19-related spatial covariance pattern.[3] All processing steps were implemented with an in-house pipeline in MATLAB (The MathWorks, Inc., Natick, Massachusetts, USA) and SPM12 software (https://www.fil.ion.ucl.ac.uk/spm/software/download/).

Statistical analysis

Statistical analyses were performed using R (https://www.R-project.org/) and SPSS version 25 (IBM). Shapiro-Wilk and Kolmogorov-Smirnov tests were used to assess normal distribution of data. For group comparisons, ANCOVAs were carried out with covariates 'age' and 'sex'. The association between V-CSF and dependent variables (i.e. MoCA-performance, olfactory performance and PES of the COVID-19 related spatial covariance pattern of cerebral glucose metabolism) was examined using partial Pearson's correlations controlling for age and sex. Tests were performed using Bonferroni correction for multiple comparisons.

Data availability

Data and code are available from the authors upon reasonable request.

Results

Patient characteristics

We report structural MRI data and cognitive performance of a cohort of 20 subacute COVID-19 patients. Demographics, patient characteristics and reasons for cerebral imaging are listed in Table 1 and the Supplementary material. Of those, 14/20 patients underwent cerebral ^{18}F-FDG PET. Regarding MoCA performance, 14 of 20 patients (70%) performed below the cut-off score for cognitive impairment (<26/30).[20] The group mean (± SD) MoCA score was 22.4 ± 4.9. The MoCA domain scores revealed particular impairment in the domains of executive abilities, visuoconstruction, memory and attention (Table 1) whereas language and orientation were not impaired. The detailed neuropsychological test battery that was available for a subset of patients largely corroborated this predominant impairment of executive function, attention and memory (Supplementary material). Olfactory performance was impaired (≤10/12 correctly identified odours) in 19 of 20 patients (95%). The mean performance of the group was 7.7 ± 1.7.

Visual evaluation of structural MRI

Subacute pinhead-sized micro-embolic infarctions were observed in 4/20 patients (bilateral cerebellar; right corona radiata; left superior cerebellar peduncle and the right frontal cortex). Old micro-embolic lesions were observed in 3/20 patients and microangiopathic white matter changes were present in 6/20 patients ($n = 1$ Fazekas 1, $n = 4$ Fazekas 2, and $n = 1$ with Fazekas 3).[32] In one patient, a small non-space-occupying meningioma at the vertex was detected. Beyond that, no other structural changes, signs of atrophy or any evidence of inflammation (e.g. leptomeningeal enhancement) were found.

COVID-19-related changes of white matter DMI parameters

A comparison of whole-brain white matter DMI parameters between COVID-19 patients and controls was performed using ANCOVAs controlling for 'age' and 'sex' (Fig. 1). In COVID-19 patients, a significant reduction of V-intra ($P = 0.032$; df: 51; $t = 2.20$; Cohen's d: 0.30) and V-extra ($P = 0.013$; df: 51; $t = 2.56$; Cohen's d: 0.35) could be detected. Consequently, a highly significant increase in V-CSF ($P < 0.001$; df: 51, $t = -4.02$; Cohen's d: 0.541) was present in COVID-19 patients indicating a volume shift into the V-CSF. In consistence with DMI results, a significant increase of whole-brain white matter V_{iso}, the homologue of V-CSF was observed using the AMICO-NODDI approach (Supplementary material). As the three compartment model defines '1 = V-CSF + V-intra + V-extra' (i.e. connecting V-CSF changes to inverse changes of V-intra + V-extra by definition), we restricted further analyses to the parameter V-CSF only. To display the weights and spatial distribution of the overall significant 'COVID-19-related effect' on V-CSF, we extracted the standardized regression coefficients (beta) of the factor

Table 1 Characteristics of COVID-19 patients

COVID-19 patients ($n = 20$)	
Demographic data	***n* (%) or mean (SD); range**
Age (years)	57.3 (17.1); 20 to 89
Sex (male/female)	16 (80)/4 (20)
Δ positive PCR: clinical examination (days)	25.5 (17.6); 2 to 69
Δ positive PCR: cMRT (days)	29.3 (14.8); 10 to 69
Δ positive PCR: ^{18}F-FDG-PET (days)	29.8 (8.9); 16 to 43
Main reason for inpatient treatment	***n* (%)**
Bacterial pulmonary superinfection	5 (25%)
Ischaemic stroke	1 (5%)
Kidney failure	3 (15%)
Malignancies	3 (15%)
Reduced general condition	7 (35%)
Seizures	1 (5%)
Treatment modality	***n* (%)**
No ICU treatment	15 (75%)
ICU without ventilation	4 (20%)
ICU with ventilation	1 (5%)
Reason for cerebral imaging	***n* (%)**
Subacute cognitive impairment	11 (55%)
Cranial nerve palsy	3 (15%): 1 N. III, 1 N. VII, 1 N. VIII
Delirium	2 (10%)
Suspicion of ischaemic stroke	2 (10%)
Retinal infarction	1 (5%)
Seizures	1 (5%)
Comorbidities	***n* (%)**
Atrial fibrillation	2 (10%)
Chronic pulmonary obstructive disease	1 (5%)
Coronary heart disease	4 (20%)
Diabetes mellitus	3 (15%)
Generalized sarcoidosis (no CNS affection)	1 (5%)
Hypercholesterolaemia	5 (25%)
Hypertension	11 (55%)
Immunosuppression	4 (20%)
Corticosteroids	4 (20%)
Tacrolimus	2 (10%)
Mycophenolate mofetil	2 (20%)
Kidney transplantation	2 (10%)
Peripheral arterial occlusive disease	1 (5%)
Pulmonary embolism	1 (5%)
Clinical readouts	**Mean (SD); range**
MoCA sum score (corrected for years of education)	22.4 (4.9); 11 to 29
MoCA domain scores	
Orientation (max. 6 points)	5.74 (0.56); 4 to 6
Attention (max. 6 points)	4.74 (1.56); 1 to 6
Language (max. 5 points)	4.63 (0.68); 3 to 5
Executive (max. 4 points)	2.63 (0.96); 1 to 4
Visuoconstructive (max. 4 points)	2.21 (1.32); 0 to 4
Memory (max. 5 points)	1.89 (1.70); 0 to 5
Correct perception of smell (12 items)	7.7 (1.7); 5 to 11
Peak IL-6 values (pg/ml)	50.5 (51.9); 1.5 to 187

cMRT = cranial magnetic resonance tomography; N. III/VII/VIII = oculomotor/facial/vesibular nerves.

V-CSF from regression models attained by voxel-wise comparisons between COVID-patients and controls (with nuisance covariates 'age', 'sex' and 'tissue probability value'). Standardized regression coefficients as a measure of effect size indicate a widespread increase of V-CSF with maxima in the frontal and parietal white matter (Fig. 2).

Displaying the network of most affected white matter fibres

To further capture the network of streamlines that were especially affected by COVID-19-related V-CSF increase, we calculated a regression model attained by streamline-wise comparisons between COVID-patients and controls (with nuisance covariates 'age' and 'sex') using an explorative threshold of $P < 0.001$. Resulting fibres are displayed in Fig. 3A. Three dimensional streamlines were further rendered to generate a visiting map (Fig. 3B) allowing an alignment with a probabilistic white matter atlas[29] (Table 2). Thus, large parts of supratentorial white matter tracts were affected by COVID-19-related changes.

Relating V-CSF to clinical parameters and cerebral metabolism

The association of V-CSF within the whole white matter to clinical outcomes and glucose metabolism was assessed using a partial Pearson's correlation approach controlling for sex and age as covariates (Fig. 4A). Regarding MoCA-performance, a highly significant inverse correlation was present ($r = -0.64$; $P = 0.006$). For IL-6, a non-significant trend towards a positive correlation with V-CSF was present ($r = 0.48$; $P = 0.068$). With respect to olfactory performance, no significant association could be detected ($r = 0.29$; $P = 0.12$). To address the possibility that only local alterations within the frontobasal white matter (z −15 to −22) could be associated with impaired smell, we assessed the relation between olfactory performance and volume fractions within this particular area. Here, V-CSF was also not correlated with olfactory performance ($r = 0.14$, $P = 0.57$). Regarding the changes of cerebral glucose metabolism, a significant correlation between whole-brain white matter V-CSF and the PES of the COVID-19 related spatial covariance pattern on ^{18}F-FDG PET was found ($r = 0.57$; $P = 0.039$). Interestingly, V_{iso} (i.e. the AMICO-NODDI homologue of V-CSF) was similarly associated to clinical outcomes and the PES of the COVID-19 related covariance pattern (Supplementary material). To further demonstrate spatial distribution of cortical regions most pronounced by COVID-19 related covariance pattern, the highest quartile of negative voxel weights (i.e. relative hypometabolism) was displayed in Fig. 4B. Frontoparietal emphasis of COVID-19-related changes was reflected both by V-CSF increase and covariance pattern of glucose metabolism.

Discussion

Widespread microstructural alterations were detected in subacute COVID-19 patients using a novel DMI approach. In summary, a redistribution with decreasing intraaxonal and extraaxonal volume fractions (V-intra and V-extra) and an increasing free water/CSF (V-CSF) fraction was observed, in line with vasogenic 0edema.[17] This diffuse process with maxima in the frontal and parietal white matter affected large parts of the supratentorial fibre tracts. As there was a non-significant trend for an association between V-CSF and peak levels of IL-6, systemic inflammation may be the trigger of these changes. The magnitude of V-CSF-increase was tightly associated with cognitive impairment, as expressed by low MoCA performance. In turn, the lack of association between white matter alterations and olfactory performance may suggest a peripheral rather than central mechanism for COVID-19-related disturbance of smell. The extent of V-CSF was also positively correlated with the expression of the previously established

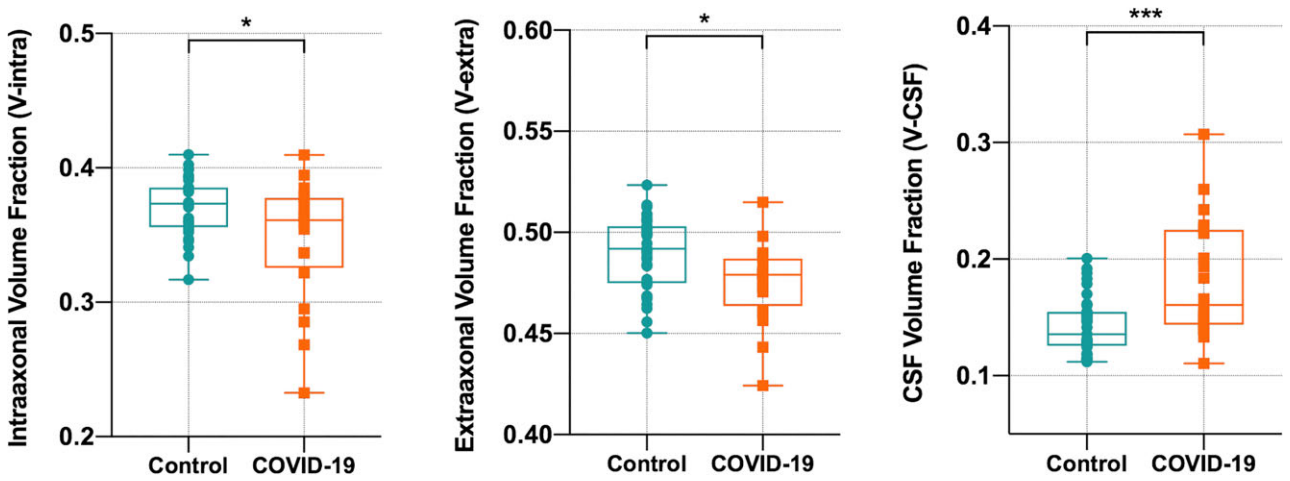

Figure 1 Comparison of whole white matter DMI parameters between COVID-19 patients and controls. Box plots show the distribution of volume fractions within the entire white matter. In COVID-19 patients, a significant decrease of V-intra and V-extra was accompanied by a highly significant increase of V-CSF. Thus, there is a global volume shift from intra- and extra-axonal space into the V-CSF. Group comparisons were performed by ANCOVAs with covariates 'age' and 'sex'. *$P < 0.05$; ***$P < 0.001$.

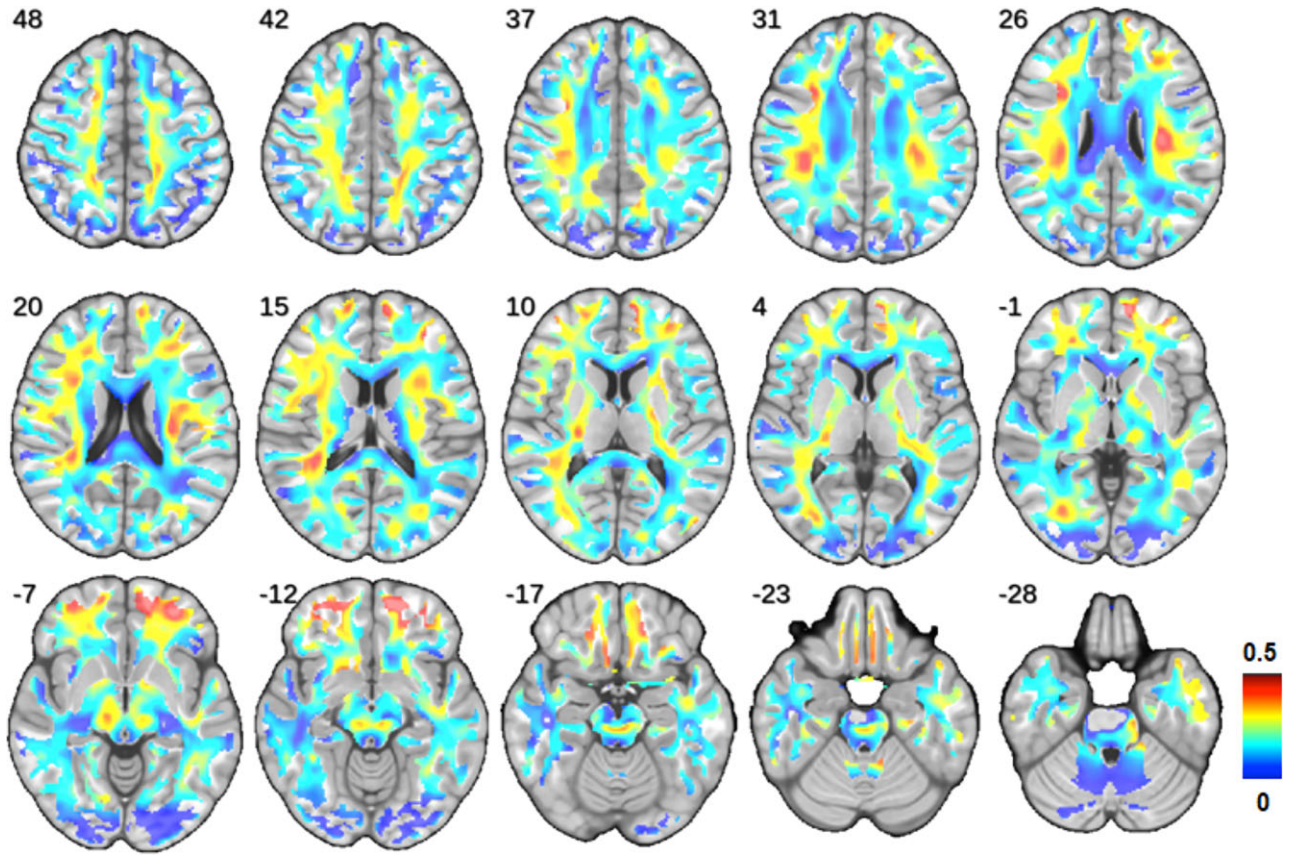

Figure 2 Spatial distribution and weights of COVID-19-related changes. The standardized regression coefficients of the factor V-CSF were extracted from regression models attained by voxel-wise comparisons between COVID-19 patients and controls (with covariates 'age', 'sex' and 'tissue probability value') and were superimposed onto a T_1-weighted MRI template. Colour-coding indicates the coefficient values as a measure of effect size of the factor 'COVID-19' on V-CSF (hot colours: large effect size versus cold colours: small effect size). Please note that all coefficients monodirectionally indicated an increase in V-CSF. Radiological orientation, i.e. left image side corresponds to patient's right body side; numbers denote the axial (z) position in millimetres.

COVID-19-related spatial metabolic covariance pattern[3] in a subgroup of patients that also underwent ^{18}F-FDG PET imaging. Likewise, the frontoparietal-dominant pattern of neocortical glucose hypometabolism is in good agreement with the frontal and parietal focus of V-CSF increase. Finally, the pattern of affected MoCA-domains (impairment in executive function, memory and

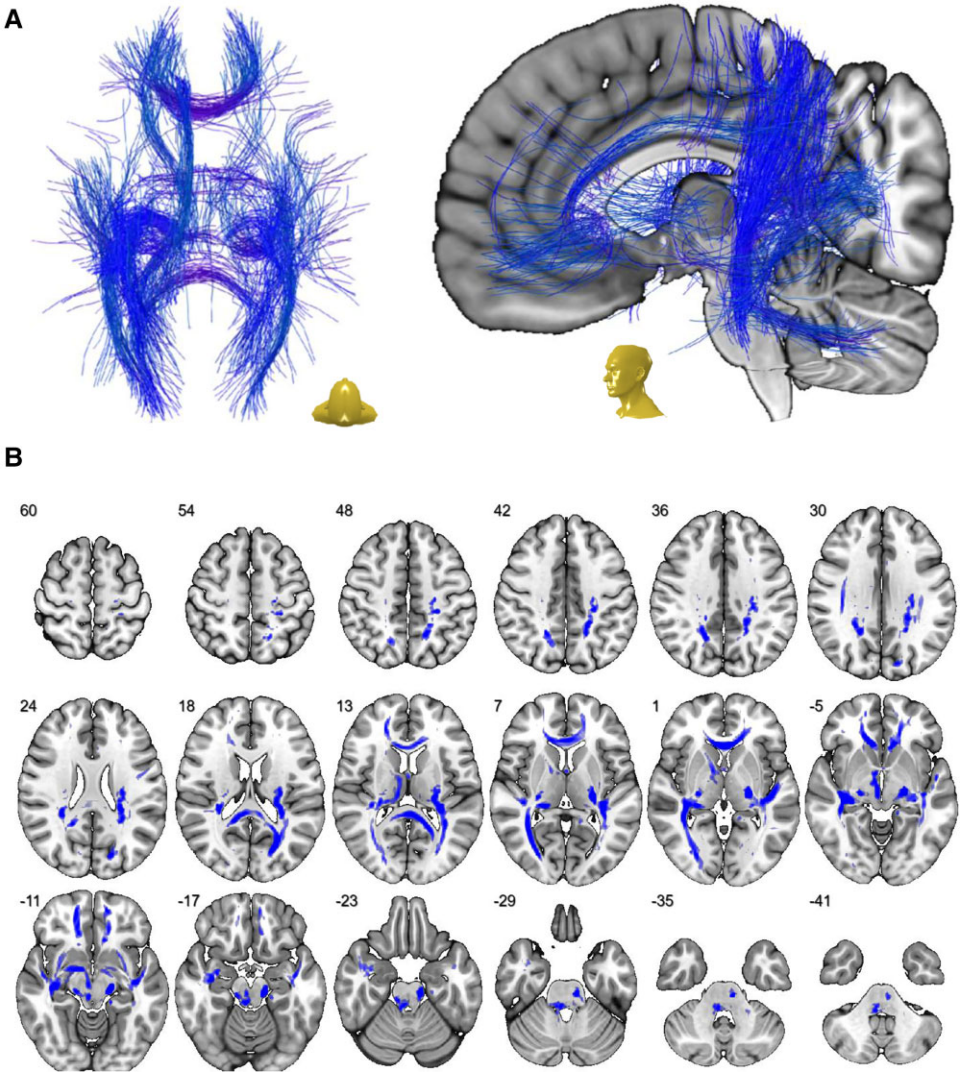

Figure 3 Network of most affected white matter fibres. (**A**) Streamline-wise comparisons between COVID-19 patients and controls (with nuisance covariates 'age' and 'sex'; exploratory threshold of $P < 0.001$) reveal a widespread network of white matter fibres in MNI space that were most affected by COVID-19-related V-CSF increase. (**B**) To display the distribution and extent of the aforementioned network in the white matter, 3D streamlines were rendered to generate a visiting map in MNI space (blue shading) that is superimposed onto a transversal T_1-weighted template. Depicted in radiological orientation, i.e. left image side corresponds to patient's right body side; numbers denote the axial (z) position in millimetres.

visuoconstruction) is in line with the frontoparietal emphasis of white matter changes and glucose hypometabolism.

Neuropathological investigations in patients who died from COVID-19 point to an inflammatory affection of the white rather than the grey matter.[5,6] Thus, we hypothesized a disturbance of white matter fibres resulting in a decreased activation of adjacent cortical regions, probably due to an impairment of afferent inputs.[3] In line with this hypothesis, the patterns of COVID-19-related changes on V-CSF and metabolism were both characterized by a frontoparietal accent. The spatial distribution of COVID-19-related V-CSF increase has to be furthermore aligned with white matter microstructure, especially the perivascular spaces (PVS). Although we did not perform a delineation of these structures based on our dataset, the spatial distribution of PVS is known from various studies using different MRI-based approaches in healthy subjects and under pathological conditions.[33–38] The highest density of PVS can be detected within the centrum semiovale (also with a frontoparietal emphasis), basal ganglia and midbrain, in good agreement with the maximal effect size of the factor 'COVID-19' on V-CSF (i.e. Fig. 2). Thus, maxima of V-CSF increase were present in white matter regions with a high density of perivascular spaces. Importantly, the role of this perivascular compartment as a key site of immune activation specific for COVID-19 has been recently identified.[5] Here, infiltration of CD8 and CD4T cells could be observed in association with blood–brain barrier dysfunction. CD8 T cells further migrate into the parenchymal compartment and are even present in microglia nodules. Therefore, widespread parenchymal glia activation[4,6] likely depends on T-cell-microglial interactions enrooted in a perivascular activation of adaptive immunity.[5] In general, vasogenic oedema due to volume shifts into perivascular space results from up-regulation of aquaporin-4 (AQP4)-water channels in (T-cell mediated) activated astrocytes in response to an inflammatory stimulus.[39,40] Fibrinogen extravasation as a sign of vascular leakage and increased blood brain barrier-permeability has been also detected in patients that died from COVID-19.[5] The consecutive enlargement of perivascular

Table 2 Distribution of COVID-related pathology derived by probabilistic atlases of white matter regions

Atlas region (white matter)	Overlap with atlas region (%)
Corticospinal tract	53
Inferior cerebellar peduncle	42
Medial lemniscus	86
Superior cerebellar peduncle	52
Cerebral peduncle	55
Anterior limb of internal capsule	36
Posterior limb of internal capsule	58
Posterior thalamic radiation	68
Anterior corona radiata	51
Superior corona radiata	26
Posterior corona radiata	84
Cingulum (cingulate gyrus)	30
Cingulum (hippocampus)	21
Fornix(cres) Stria terminalis	39
Superior longitudinal fasciculus	47
Superior frontooccipital fasciculus	23
Inferior frontooccipital fasciculus	47
Sagittal stratum	40
External capsule	20
Uncinate fasciculus	46
Pontine crossing tract	41
Middle cerebellar peduncle	18
Fornix	27
Genu of corpus callosum	76
Body of corpus callosum	8
Splenium of corpus callosum	57
Retrolenticular part of internal capsule	94
Tapatum	25

spaces should result in increased V-CSF volume fractions particularly in regions with a high density of these structures. In addition to vasogenic oedema, occurrence of cytotoxic oedema has been described in infectious encephalitis.[41] As cytotoxic oedema results from swelling of stalling neurons and neurites, an increment of the intracellular volume fraction should be expected. As neuropathology failed to detect a relevant amount of lytic neurons and glia[4–6] and V-intra significantly decreased, cytotoxic oedema seems to play a minor role in our COVID-19 cohort.

Moreover, it is worth considering that altered DMI-parameters may also indicate (irreversible) axonal damage. In line with this theory, elevated concentrations of neurofilament light chain, a marker of axonal injury, have been detected in serum[42,43] and CSF[44] of COVID-19 patients and were discussed as markers for an adverse outcome.[45] Likewise, the decrease of whole white matter V-intra observed in this study may also point to reduced fibre integrity as observed due to chronic inflammation[18] or mechanical stress.[19] However, as V-CSF increase coincides with the spatial distribution of perivascular spaces and is associated with IL-6 peak values at trend level, the analysis of DMI-parameters likely captured post-inflammatory volume redistributions rather than measuring axonal damage in white matter fibre networks. Due to the cross-sectional design of our present work, we cannot demonstrate longitudinal development of DMI-parameters. However, few studies (including a follow-up investigation of patients from our cohort[3]) provide longitudinal data on cerebral glucose metabolism assessed by ^{18}F-FDG PET and cognitive impairments,[30,46,47] both being significantly associated with V-CSF in our cross-sectional data. Here, cortical dysfunction and cognitive deficits were grossly reversible, albeit minor residuals may still be present six months after COVID-19. This implies that changes in white matter microstructure are unlikely to result from irreversible structural damage. On the other hand, the risk of being diagnosed with dementia or parkinsonism 6 months after infection is larger in COVID-19 compared to influenza or other respiratory tract infections.[2] This is especially the case for patients with a severe course of disease and those suffering from an encephalopathy in the acute phase. Likewise, a post-mortem transcriptomic analysis of frontal cortex tissue of patients that died from COVID-19 revealed a molecular signature of ageing (i.e. downregulation of genes involved in synaptic function and cognition and upregulation of genes involved in immune processes) compared to controls.[48] Thus, COVID-19 may accelerate degenerative or aging processes in a subset of patients (severe course of disease, encephalopathy).

To date, structural MRI studies of COVID-19 patients revealed a broad spectrum of brain abnormalities including leukoencephalopathy, microhaemorrhages, neurovascular complications and inflammatory or posterior reversible encephalopathy syndrome (PRES)-like syndromes.[7,8] In a large longitudinal MRI study from the UK Biobank that compared pre- with post-COVID-19 scans (on average four to five months after infection), an increase of diffusion indices as markers of tissue damage was detected in regions connected to the olfactory cortex (i.e. piriform cortex, olfactory tubercle and anterior olfactory nucleus).[49] Moreover, a reduction in global measures of brain size and increase in cerebrospinal fluid volume was present in COVID-19 patients suggesting accelerated diffuse atrophy. Although the Trail Making Test revealed larger decline compared to controls, no further information on neurological symptoms or olfactory performance was present in this dataset. In a cross-sectional study investigating 190 COVID-19 patients with neurological symptoms, only 20% of scans revealed abnormal findings (excluding infarctions and cerebral venous thrombosis).[9] In another smaller series of six patients with respiratory failure and severe neurological symptoms (e.g. persistent unresponsiveness after washout of sedative agents), structural MRI revealed no seminal pathology.[10] Moreover, although neuropathological changes are frequent in patients who died from COVID-19,[4,6] only ~20% of post-mortem MRI scans of COVID-19 patients show potentially COVID-19-related imaging abnormalities.[11] To overcome this obvious gap between clinical symptoms, (histo-)pathology and structural MRI, diffusion MRI was chosen as a promising approach to provide information exceeding the pure macrostructure. Indeed, significant reduction of fractional anisotropy in various white matter tracts has been detected in patients after mild and severe COVID-19 infection without any neurological manifestations three months after symptom onset.[50] Moreover, widespread fractional anisotropy reduction was observed in 28 COVID-19 patients 3 months after discharge using tract-based spatial statistics.[51] Although reduced fractional anisotropy has been interpreted as a sign of white matter injury in both studies, the increased mean and radial diffusivity detected in the study of Yang and colleagues would be more compatible with oedema than isolated axonal damage. Also in line with our observations, in the aforementioned case series of six subacute (i.e. 3 weeks after symptom manifestation) COVID-19 patients with severe neurological symptoms, analysis of DTI parameters revealed increased mean diffusivity within numerous white matter tracts (e.g. commissural fibres, thalamic radiation).[10] In contrast to these and our results, a study investigating 60 COVID-19 patients of a mixed population (68% with neurological symptoms), which was conducted also three month after symptom onset, detected an increase in global grey matter fractional anisotropy compared to controls, whereas white matter fractional anisotropy was not different between groups.[52]

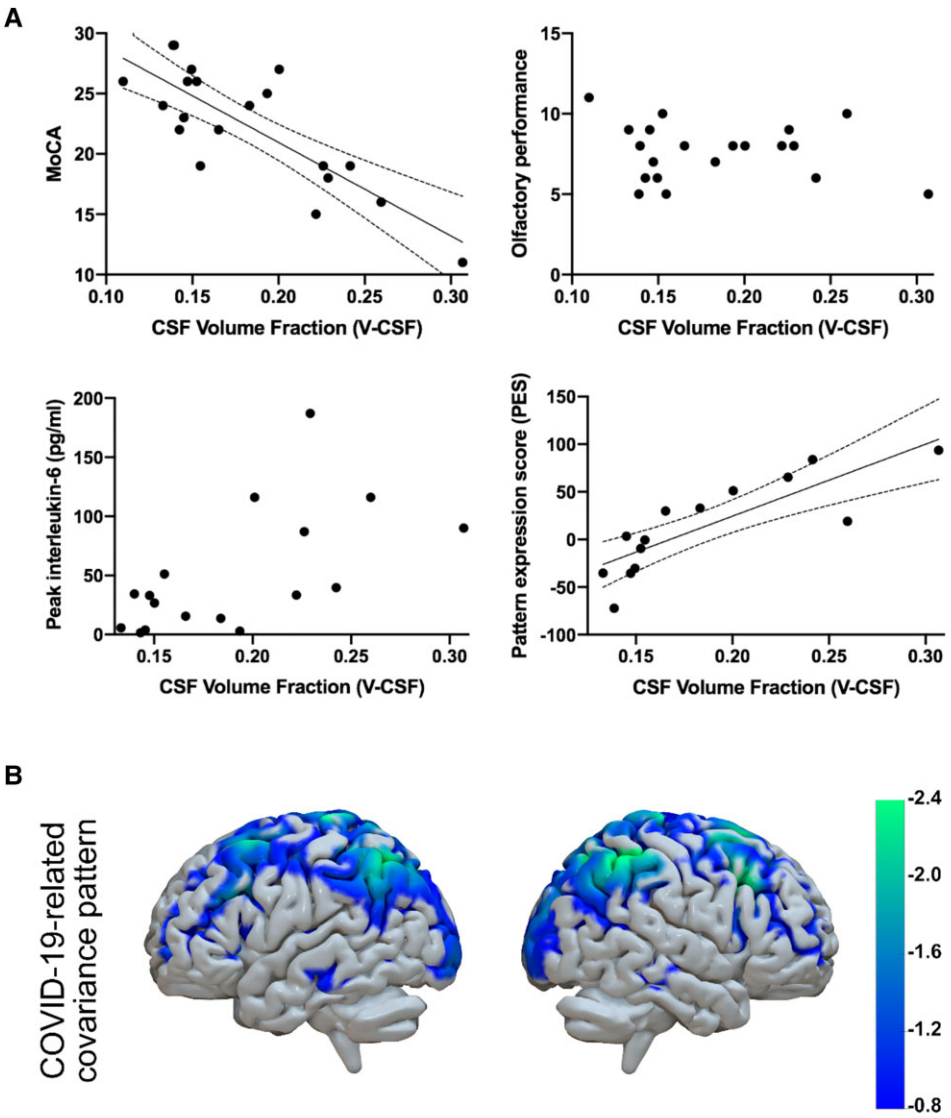

Figure 4 Association of whole white matter V-CSF with clinical parameters and cerebral glucose metabolism assessed by ^{18}F-FDG PET imaging. (**A**) Associations were assessed using partial Spearman's correlations with 'age' and 'sex' as covariates. Each dot represents an individual patient's data. In case of a significant correlation, a linear regression was fitted (black line) and dotted lines indicate the 95% confidence interval. For MoCA performance, a significant inverse correlation with V-CSF emerged. No significant correlation was present between olfactory performance and V-CSF. Between IL-6 peak values and V-CSF, a non-significant trend for a correlation was present. The pattern expression score (PES) as a measure of COVID-19-related changes in cerebral glucose metabolism was significantly correlated with V-CSF. Please note that only 14 of 23 patients underwent ^{18}F-FDG PET imaging. (**B**) COVID-19-related spatial covariance pattern of cerebral glucose metabolism established by Hosp and colleagues.[3] Displayed were voxels of the highest quartile of negative voxel weights (i.e. relative hypometabolism) overlaid onto a T_1-weighted MRI-based volume mesh.

Unlike MoCA, olfactory performance was not associated with DMI parameters. After mucosal inoculation of HCoV-OC43, another beta-coronavirus, viral invasion was shown via axonal transport along olfactory fibres in animal models.[53] In line with this view, SARS-CoV-2 RNA could be detected in nasal epithelium of patients that died from COVID-19 and, at considerably lower levels, in olfactory bulb tissue.[6] Neuroinflammation was furthermore detected within olfactory bulb tissue, although the pattern of immune activation clearly differed from that observed in the brainstem.[5] Unfortunately, we were not able to investigate the olfactory tract due to susceptibility artefacts close to the base of the skull and its small volume. In the aforementioned longitudinal study of the UK Biobank, the affection of regions connected to the olfactory cortex (i.e. piriform cortex, olfactory tubercle, anterior olfactory nucleus, left parahippocampal gyrus and orbitofrontal cortex) points to an involvement of the central olfactory system.[49] However, as the authors discuss, these changes were not necessarily caused by direct viral damage but may be consequence of secondary deprivation processes. The lack of correlation between V-CSF in orbitofrontal white matter and olfactory performance may argue for the latter hypothesis. In addition, viral affection of olfactory epithelial support cells could have contributed to olfactory dysfunction independently from neural processes.[54]

Several limitations have to be taken into account for the interpretation of the present study. Due to its cross-sectional design and the lack of a 'pre-COVID-19' MRI, a cause-effect relationship between COVID-19 and changes in diffusivity parameters cannot be proven. Furthermore, the detected changes could be a non-specific

consequence of a reduced general condition in critically ill patients. However, MRI scans were performed 3 to 4 weeks after positive SARS-CoV-2-PCR, a time point when patients had surmounted COVID-19 symptoms (e.g. fever, cough, dyspnoea) and were close to discharge from hospital. In addition, the larger burden of co-morbidities in COVID-19 patients could be seen as a source of confound. The substantial reversibility of cortical dysfunction and cognitive deficits,[30,46,47] factors tightly coupled to V-CSF increase, however argue against a major impact of such static factors. Lastly, as we did not include respective control groups (e.g. hospitalized patients diagnosed with influenza or other respiratory tract infections) we cannot state if the increase if V-CSF is specific for COVID-19 or not (in fact, on first glace this appears unlikely, given the postulated non-specific mechanism). Regarding our statistical models, age[55] and sex[56] were included as nuisance covariates, assuming a possible linear relationship to diffusivity parameters. Still, our approach is necessarily a simplistic approximation, given that the type of relationship (linear versus non-linear) differs among particular white matter tracts[55] and that we were not able to apply non-linear models because of the limited sample size.

Acknowledgements

The use in this work of ScAnVP software, copyright © 2021 The Feinstein Institute for Medical Research, is hereby acknowledged.

Funding

N.S. is supported by the Berta-Ottenstein-Programme for Clinician Scientists, Faculty of Medicine, University of Freiburg. A.D. is supported by the Berta-Ottenstein-Programme for Advanced Clinician Scientists, Faculty of Medicine, University of Freiburg.

Competing interests

P.T.M. received honoraria for lectures and consulting by GE and Philips. H.U. is co-editor of Clinical Neuroradiology, member of the Advisory Board of Biogen and received honoraria for lectures from Biogen, Eisai, and mbits. E.K. is shareholder of and received fees from VEObrain GmbH, Freiburg, Germany N.S. received honoraria for lectures sponsored by Abbvie. All other authors report no competing interests.

Supplementary material

Supplementary material is available at *Brain* online.

References

1. Paterson RW, Brown RL, Benjamin L, *et al*. The emerging spectrum of COVID-19 neurology: clinical, radiological and laboratory findings. *Brain*. 2020;143:3104–3120.
2. Taquet M, Geddes JR, Husain M, Luciano S, Harrison PJ. 6-month neurological and psychiatric outcomes in 236 379 survivors of COVID-19: a retrospective cohort study using electronic health records. *Lancet Psychiatry*. 2021;8(5):416–427.
3. Hosp JA, Dressing A, Blazhenets G, *et al*. Cognitive impairment and altered cerebral glucose metabolism in the subacute stage of COVID-19. *Brain*. 2021;144:1263–1276.
4. Matschke J, Lütgehetmann M, Hagel C, *et al*. Neuropathology of patients with COVID-19 in Germany: a post-mortem case series. *Lancet Neurol*. 2020;19(11):919–929.
5. Schwabenland M, Salié H, Tanevski J, *et al*. Deep spatial profiling of human COVID-19 brains reveals neuroinflammation with distinct microanatomical microglia-T-cell interactions. *Immunity*. 2021;54(7):1594–1610.e11.
6. Thakur KT, Miller EH, Glendinning MD, *et al*. COVID-19 neuropathology at Columbia University Irving Medical Center/New York Presbyterian Hospital. *Brain*. 2021;144:2696–2708.
7. Choi Y, Lee MK. Neuroimaging findings of brain MRI and CT in patients with COVID-19: a systematic review and meta-analysis. *Eur J Radiol*. 2020;133:109393.
8. Gulko E, Oleksk ML, Gomes W, *et al*. MRI brain findings in 126 patients with COVID-19: initial observations from a descriptive literature review. *AJNR Am J Neuroradiol*. 2020;41(12):2199–2203.
9. Kremer S, Lersy F, de Sèze J, *et al*. Brain MRI findings in severe COVID-19: a retrospective observational study. *Radiology*. 2020;297(2):E242–E251.
10. Newcombe VFJ, Spindler LRB, Das T, *et al*. Neuroanatomical substrates of generalized brain dysfunction in COVID-19. *Intensive Care Medicine*. 2021;47(1):116–118.
11. Coolen T, Lolli V, Sadeghi N, *et al*. Early postmortem brain MRI findings in COVID-19 non-survivors. *Neurology*. 2020;95(14):e2016–e2027.
12. Kamiya K, Hori M, Aoki S. NODDI in clinical research. *J Neurosci Methods*. 2020;346:108908.
13. Novikov DS, Reisert M, Kiselev VG. Effects of mesoscopic susceptibility and transverse relaxation on diffusion NMR. *J Magn Reson*. 2018;293:134–144.
14. Reisert M, Kellner E, Dhital B, Hennig J, Kiselev VG. Disentangling micro from mesostructure by diffusion MRI: a Bayesian approach. *Neuroimage*. 2017;147:964–975.
15. Zhang J, Zhang Y, Xing S, Liang Z, Zeng J. Secondary neurodegeneration in remote regions after focal cerebral infarction: a new target for stroke management? *Stroke*. 2012;43(6):1700–1705.
16. Broad RJ, Gabel MC, Dowell NG, *et al*. Neurite orientation and dispersion density imaging (NODDI) detects cortical and corticospinal tract degeneration in ALS. *J Neurol Neurosurg Psychiatry*. 2019;90(4):404–411.
17. Palacios EM, Owen JP, Yuh EL, *et al*. The evolution of white matter microstructural changes after mild traumatic brain injury: a longitudinal DTI and NODDI study. *Sci Adv*. 2020;6(32):eaaz6892.
18. Margoni M, Petracca M, Schiavi S, *et al*. Axonal water fraction as marker of white matter injury in primary-progressive multiple sclerosis: a longitudinal study. *Eur J Neurol*. 2019;26:1068–1074.
19. By S, Xu J, Box BA, Bagnato FR, Smith SA. Application and evaluation of NODDI in the cervical spinal cord of multiple sclerosis patients. *NeuroImage Clin*. 2017;15:333–342.
20. Nasreddine ZS, Phillips NA, Bédirian V, *et al*. The Montreal Cognitive Assessment, MoCA: a brief screening tool for mild cognitive impairment. *J Am Geriatr Soc*. 2005;53(4):695–699.
21. Kobal G, Hummel T, Sekinger B, Barz S, Roscher S, Wolf S. 'Sniffin' sticks': screening of olfactory performance. *Rhinology*. 1996;34(4):222–226.
22. Shekhawat J, Gauba K, Gupta S, *et al*. Interleukin-6 perpetrator of the COVID-19 cytokine storm. *Indian J Clin Biochem*. 2021;36:1–11.
23. Veraart J, Novikov DS, Christiaens D, Ades-Aron B, Sijbers J, Fieremans E. Denoising of diffusion MRI using random matrix theory. *Neuroimage*. 2016;142:394–406.
24. Kellner E, Dhital B, Kiselev VG, Reisert M. Gibbs-ringing artifact removal based on local subvoxel-shifts. *Magn Reson Med*. 2016;76(5):1574–1581.

25. Zhang H, Schneider T, Wheeler-Kingshott CA, Alexander DC. NODDI: practical in vivo neurite orientation dispersion and density imaging of the human brain. *Neuroimage*. 2012;61(4):1000–1016.
26. Daducci A, Canales-Rodríguez EJ, Zhang H, Dyrby TB, Alexander DC, Thiran JP. Accelerated Microstructure Imaging via Convex Optimization (AMICO) from diffusion MRI data. *NeuroImage*. 2015;105:32–44.
27. Ashburner J. A fast diffeomorphic image registration algorithm. *Neuroimage*. 2007;38(1):95–113.
28. Reisert M, Mader I, Anastasopoulos C, Weigel M, Schnell S, Kiselev V. Global fiber reconstruction becomes practical. *Neuroimage*. 2011;54(2):955–962.
29. Hua K, Zhang J, Wakana S, *et al*. Tract probability maps in stereotaxic spaces: analyses of white matter anatomy and tract-specific quantification. *Neuroimage*. 2008;39(1):336–347.
30. Blazhenets G, Schroeter N, Bormann T, *et al*. Slow but evident recovery from neocortical dysfunction and cognitive impairment in a series of chronic COVID-19 patients. *J Nucl Med*. 2021;62(7):910–915.
31. Spetsieris P, Ma Y, Peng S, *et al*. Identification of disease-related spatial covariance patterns using neuroimaging data. *J Vis Exp*. 2013;76:50319.
32. Fazekas F, Chawluk JB, Alavi A, Hurtig HI, Zimmerman RA. MR signal abnormalities at 1.5T in Alzheimer's dementia and normal aging. *AJR Am J Roentgenol*. 1987;149(2):351–356.
33. Sepehrband F, Barisano G, Sheikh-Bahaei N, *et al*. Volumetric distribution of perivascular space in relation to mild cognitive impairment. *Neurobiol Aging*. 2021;99:28–43.
34. Donahue EK, Murdos A, Jakowec MW, *et al*. Global and regional changes in perivascular space in idiopathic and familial Parkinson's disease. *Mov Disord*. 2021;36(5):1126–1136.
35. Barisano G, Law M, Custer RM, Toga AW, Sepehrband F. Perivascular space imaging at ultrahigh field MR imaging. *Magn Reson Imaging Clin N Am*. 2021;29(1):67–75.
36. Feldman RE, Rutland JW, Fields MC, *et al*. Quantification of perivascular spaces at 7T: a potential MRI biomarker for epilepsy. *Seizure*. 2018;54:11–18.
37. Dubost F, Yilmaz P, Adams H, *et al*. Enlarged perivascular spaces in brain MRI: automated quantification in four regions. *NeuroImage*. 2019;185:534–544.
38. Barisano G, Sheikh-Bahaei N, Law M, Toga AW, Sepehrband F. Body mass index, time of day and genetics affect perivascular spaces in the white matter. *J Cereb Blood Flow Metab*. 2021;41(7):1563–1578.
39. Filiano AJ, Gadani SP, Kipnis J. How and why do T cells and their derived cytokines affect the injured and healthy brain? *Nat Rev Neurosci*. 2017;18(6):375–384.
40. Mogensen FLH, Delle C, Nedergaard M. The glymphatic system (en)during inflammation. *Int J Mol Sci*. 2021;22(14):7491.
41. Dalby T, Wohl E, Dinsmore M, Unger Z, Chowdhury T, Venkatraghavan L. Pathophysiology of cerebral edema—a comprehensive review. *J Neuroanaesthesiol Crit Care*. 2021;8:163–172.
42. Ameres M, Brandstetter S, Toncheva AA, *et al*. Association of neuronal injury blood marker neurofilament light chain with mild-to-moderate COVID-19. *J Neurol*. 2020;267(12):3476–3478.
43. Kanberg N, Ashton NJ, Andersson LM, *et al*. Neurochemical evidence of astrocytic and neuronal injury commonly found in COVID-19. *Neurology*. 2020;95:e1754–e1759.
44. Garcia MA, Barreras PV, Lewis A, *et al*. Cerebrospinal fluid in COVID-19 neurological complications: Neuroaxonal damage, anti-SARS-Cov2 antibodies but no evidence of cytokine storm. *J Neurol Sci*. 2021;427:117517.
45. Prudencio M, Erben Y, Marquez CP, *et al*. Serum neurofilament light protein correlates with unfavorable clinical outcomes in hospitalized patients with COVID-19. *Sci Transl Med*. 2021;13-(602):eabi7643.
46. Kas A, Soret M, Pyatigoskaya N, *et al*. The cerebral network of COVID-19-related encephalopathy: a longitudinal voxel-based 18F-FDG-PET study. *Eur J Nucl Med Mol Imaging*. 2021;48:2543–2557.
47. Zhao S, Shibata K, Hellyer PJ, *et al*. Rapid vigilance and episodic memory decrements in COVID-19 survivors. *medRxiv*. [Preprint] doi:10.1101/2021.07.06.21260040
48. Mavrikaki M, Lee JD, Solomon IH, Slack FJ. Severe COVID-19 induces molecular signatures of aging in the human brain. *medRxiv*. [Preprint] doi:10.1101/2021.11.24.21266779
49. Douaud G, Lee S, Alfaro-Almagro F, *et al*. Brain imaging before and after COVID-19 in UK Biobank. *medRxiv*. [Preprint] doi:10.1101/2021.06.11.21258690
50. Qin Y, Wu J, Chen T, *et al*. Long-term microstructure and cerebral blood flow changes in patients recovered from COVID-19 without neurological manifestations. *J Clin Invest*. 2021;131(8):147329.
51. Yang L, Zhou M, Li L, *et al*. Characteristics of mental health implications and plasma metabolomics in patients recently recovered from COVID-19. *Transl Psychiatry*. 2021;11(1):307.
52. Lu Y, Li X, Geng D, *et al*. Cerebral micro-structural changes in COVID-19 patients - an MRI-based 3-month follow-up study. *EClinicalMedicine*. 2020;25:100484.
53. Desforges M, Le Coupanec A, Dubeau P, *et al*. Human coronaviruses and other respiratory viruses: underestimated opportunistic pathogens of the central nervous system? *Viruses*. 2020;12(1):14.
54. Brann DH, Tsukahara T, Weinreb C, *et al*. Non-neuronal expression of SARS-CoV-2 entry genes in the olfactory system suggests mechanisms underlying COVID-19-associated anosmia. *Sci Adv*. 2020;6(31):eabc5801.
55. Behler A, Kassubek J, Müller HP. Age-related alterations in DTI metrics in the human brain-consequences for age correction. *Front Aging Neurosci*. 2021;13:682109.
56. Lim S, Han CE, Uhlhaas PJ, Kaiser M. Preferential detachment during human brain development: age- and sex-specific structural connectivity in Diffusion Tensor Imaging (DTI) data. *Cereb Cortex*. 2015;25(6):1477–1489.